MULTIPLE IMAGES AND LIGHT CURVES OF AN EMITTING SOURCE ON A RELATIVISTIC ECCENTRIC ORBIT AROUND A BLACK HOLE

G. BAO,[1,2] P. HADRAVA,[3] AND E. ØSTGAARD[1,4]
Received 1993 March 31; accepted 1993 October 13

ABSTRACT

The scenario of "spots" moving around a black hole has recently become of great interest and is considered to have important implications in astrophysics. Various studies to date have been limited to an emitting source on a circular orbit. This paper, however, presents some new results from the study of a bright source on an eccentric orbit. In the investigations, full relativistic effects are included without any approximations. Multiple images and light curves of the spot on the orbit with different parameters observed at infinity are shown. The results are then compared with those from circular orbits. It is argued that the recently revealed quasi-periodic oscillation in the X-ray emission of the Seyfert galaxy NGC 5548 can be explained in terms of a bright source on an eccentric orbit around a black hole. In addition, a method is introduced that can be applied directly in calculations of other astrophysical quantities such as the emission line from an accretion disk around a black hole or the variability power spectrum of collective "hot spots."
Subject headings: black hole physics — galaxies: nuclei — relativity

1. INTRODUCTION

Relativistic effects due to orbiting objects around a black hole have always been a subject of interest, as they might constitute a source of evidence for the existence of black holes. Pioneering papers on imaging by gravitational bending of light and its photometric consequences for eclipse phenomena were produced by Link (1936, 1937), the first one written even before the famous paper by Einstein (1936), usually referred to as historically the first study of lensing effects. The earliest work dealing with this problem in strong gravitational fields was done by Cunningham & Bardeen (1973), in which they studied the optical appearance of an orbiting star on a circular orbit around an extreme Kerr black hole. Since then, many other properties of the orbiting objects have been investigated, e.g., the polarization of light emitted by an orbiting spot on a circular orbit (Pineault 1977, 1980), the behavior of a spot moving on a spiral orbit inside the marginally stable orbit (Stoeger 1980). These "classical" studies are primarily of academic interest. Thanks to the European X-ray satellite *EXOSAT*, which has offered us a reliable picture of short-term X-ray variability of active galactic nuclei (AGNs) and Galactic X-ray sources through its uninterrupted "long looks" and the engagement of a large effective area of its energy detector, it is now possible to compare the theoretical predictions directly with the observational data.

The current AGN paradigm assumes that galactic nuclei contain supermassive black holes, surrounded by supermassive accretion disks. Since the angular dimensions of these nuclei are far below the threshold of angular resolution of current satellites, the study of time variability of the overall signal becomes the most promising key to understanding the nature of these objects. It is well known that the inner part of an accretion disk, from which most of the X-rays are emitted, is far from being smooth, instead, it suffers thermal, viscous or other kinds of instabilities (Shakura & Sunyaev 1976; Lightman & Eardley 1974; Lightman 1974; Pringle et al. 1973) and other hydrodynamic effects such as shocks, magnetic flares, etc. Therefore, under typical conditions, the inner part of accretion disks looks more like a group of "hot spots" orbiting the supermassive black hole. This view is supported by the observed noisy X-ray light curves of AGNs and by the fact that in some AGNs the time delay between the hard and soft X-ray variation is not evident, which implies that the hard X-ray sources must be imbedded somewhere inside the accretion disk (Fabian & George 1990) and corotate with the disk around the black hole. The disk therefore appears "clumpy." A model based on the above reasoning has recently been constructed to explain the observed X-ray variability (Abramowicz et al. 1989, 1991a, b; Zhang & Bao 1991; Wiita et al. 1991; Bao 1992; Bao & Stuchlík 1992, and references therein).

Theoretical investigations show that the collective behavior of the relativistic orbiting sources may account for the observed X-ray variability power spectrum of AGNs and Galactic X-ray sources, for example, the power-law variability spectrum. A single orbiting spot on any orbit can explain flare-like and quasi-periodic light curves of AGNs, peaks and "humps" in the variability power spectrum, for instance, the recently revealed quasi-periodic oscillation in the spectrum of NGC 5548 (Papadakis & Lawrence 1993). Models in this regard have been proposed by Abramowicz et al. (1992, 1993); by Rees (1992); and by Sikora & Begelman (1992), which differ from one another in their conception of the orbital plane of the bright object—the object moves either in the disk plane or on a plane which crosses the accretion disk.

Where specific applications are concerned, the variability power spectrum due to the relativistic spots and its signature have been investigated by Bao (1992); some efficient code for calculating various observable quantities has been presented by Karas, Vokrouhlický, & Polnarev (1992). The creation process of the object is still an open question. It could be a clump or a huge vortex in the accretion disk produced by

[1] Physics Institute, University of Trondheim, AVH, N-7055 Dragvoll, Norway.
[2] E-mail: bao.gang@avh.unit.no
[3] Astronomical Institute of the Academy of Sciences of the Czech Republic, CS-251 65 Ondřejov, Czech Republic; e-mail: Had@sunstel.asu.cas.cz
[4] E-mail: erlend.oestgaard@avh.unit.no

instabilities, as suggested by Abramowicz et al. (1992), it could also be an accreting neutron star, a white dwarf (Sandip & Bao 1992) or another black hole (Rees 1992).

Although the study on this subject has been carried out extensively, the optical appearance of a source orbiting on a relativistic eccentric orbit has never been described. The circular orbit sees to be a reasonable assumption in the case of a dense, continuous disk, whereas in the case of a disk consisting of individual blobs of matter (stars, gaseous clouds, etc.) with both the mutual interactions and the interaction with the embedding gas being negligible, the eccentric orbit appears more plausible. In the latter case, free spots could move on eccentric orbits, and special properties due to spots on the orbits are therefore worth investigating.

In this paper, we present multiple images and light curves of the spot observed at infinity. In the calculations, all relativistic effects are included. In § 2, the model is described, and the general calculation is presented; in § 3, the numerical results are given; there will then be a follow-up discussion in § 4 on the implications for NGC 5548. The formulae are given in detail in the Appendix.

2. MODEL AND CALCULATIONS

We assume that the emitting matter or the so-called "hot spot" is sufficiently small and moves on an eccentric orbit in the equatorial plane $\vartheta = \pi/2$ (see Fig. 1) around a Schwarzschild black hole with the corresponding external metric

$$ds^2 = -\left(1 - \frac{2}{r}\right)dt^2 + \frac{dr^2}{1 - 2/r} + r^2(d\vartheta^2 + \sin^2\vartheta\, d\varphi^2) \quad (1)$$

(the mass of the central black hole is taken as the unit of length). The observer is placed at rest at infinity in the direction $\vartheta = i$ (the inclination) and $\varphi = 0$ (i.e., the observer defines the beginning of the azimuthal coordinate). Photons are emitted by the orbiting source at $r = r_s$ and $\varphi = \varphi_s$, deflected by the central hole with deflection angle ϕ_∞, and arrive at the photographic plate of the observer with an impact parameter B. Due to the spherical symmetry of the spacetime, the particle motion is planar. The plane of the photon motion rotates around the line of sight in the course of the orbital motion: ϕ'
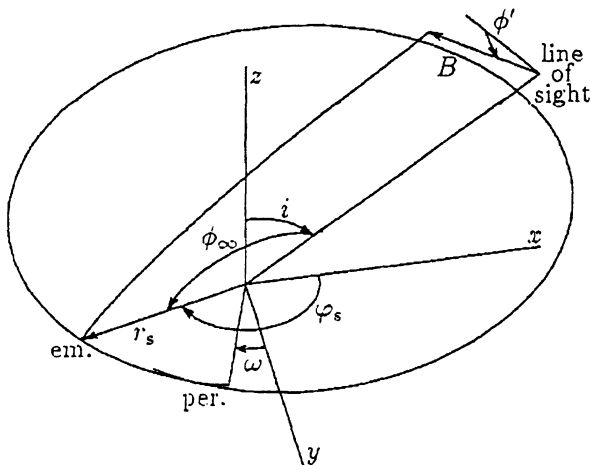

FIG. 1.—The geometry of the model

refers to its position angle; ϕ_∞ is the angle spanned by the trajectory of the direct image from the source to the observer. Both ϕ' and ϕ_∞ can be deduced from a simple geometrical consideration (see Bao 1992):

$$\sin\phi' = \frac{\sin\varphi_s}{\sqrt{1 - \cos^2\varphi_s \sin^2 i}}, \quad (2)$$

$$\cos\phi_\infty = \sin i \cos\varphi_s. \quad (3)$$

In addition, there is an infinite set of nth-order images crossing n times the line of sight. For an nth-order image,

$$\phi_{\infty,n} = \pi\left[n + \frac{1 - (-1)^n}{2}\right] + (-1)^n\phi_\infty. \quad (4)$$

On the other hand, ϕ_∞ must correspond to B through the solution of the geodesic motion

$$\phi_\infty = \int_0^{u_s} \frac{B\,du}{\sqrt{2u^3 B^2 - u^2 B^2 + 1}}, \quad (5)$$

where $u = 1/r$. From this condition, B can be calculated (see the Appendix for details). The appearance of the orbit of the source, as it could, in principle, be observed, is then described by the polar coordinates B and ϕ' on the observer's photographic plate.

The photons are supposed to be radiated isotropically in the proper rest frame of the source with the bolometric intensity I_{em}. According to geometrical optics, the bolometric intensity varies as the fourth power of the frequency along light rays, which gives the observed intensity

$$I_{obs} = g^4 I_{em}. \quad (6)$$

g is defined as the ratio of energy (E_0) at infinity to energy (E_e) in the rest frame of the emitting matter (see Cunningham & Bardeen 1973 and Misner, Thorne, & Wheeler 1973),

$$g = \frac{E_0}{E_e} = \frac{-(p \cdot u_0)_{r=\infty}}{-(p \cdot u_e)_{r=r_s}}, \quad (7)$$

where p is the four-momentum of the photon, u_e and u_0 are the four-velocities of the source and the observer. This ratio is simply related to the redshift z, defined in the usual manner, $g = (1 + z)^{-1}$ (see, e.g., Cunningham 1975). The components of the four-velocities and four-momenta can be expressed in terms of the standard constants of motion E_s and L_s (energy and angular momentum of the orbiting source on the eccentric orbit—see the Appendix) and B. The g is then given by

$$g^{-1} = \frac{r_s}{r_s - 2} E_s + r_s^{-2} B L_s \sin i \sin\phi'$$

$$- \sigma_p \sigma_s\left[\left(\frac{r_s}{r_s - 2} - r_s^{-2} B^2\right)\left(\frac{r_s}{r_s - 2} E_s^2 - 1 - r_s^{-2} L_s^2\right)\right]^{1/2}, \quad (8)$$

where σ_s and σ_p represent the orientation of the radial momenta of the source and the photon respectively: $\sigma_s = +1$ in the part from the pericenter to the apocenter; $\sigma_s = -1$ in the complementary part of the orbit; $\sigma_p = +1$ in cases (1) and (2), which are discussed in the Appendix, and $\sigma_p = -1$ in case (3).

In the case where the orbiting source spans the element $r_s \Delta r_s \Delta \varphi_s$ of the orbital plane, i.e., it radiates with the cosine-distribution of energy, the observed flux can be expressed as

$$F_{\rm obs} = I_{\rm obs} \Delta \Pi \ , \tag{9}$$

where $\Delta \Pi$ is the solid angle of the source subtended at the observer, which can be derived from

$$\Delta \Pi = \frac{B}{d^2} \left| \frac{\partial(B, \phi')}{\partial(r_s, \varphi_s)} \right| dr_s \, d\varphi_s \ , \tag{10}$$

where d is the distance from the emitting source to the observer. The Jacobian contains only two terms

$$\frac{\partial \phi'}{\partial \varphi_s} = \frac{\cos i}{1 - \sin^2 i \cos^2 \varphi_s} \ , \tag{11}$$

$$\frac{\partial r_s}{\partial B} = \frac{\sqrt{2u_s^3 - u_s^2 + B^{-2}}}{u_s^2 B^3} \int_0^{u_s} \frac{du}{(2u^3 - u^2 + B^{-2})^{3/2}} \ . \tag{12}$$

The time t of the photon's arrival at the observer should be the source travel time plus the time t_p spent by the photon moving from the source to the observer. This time has been calculated by using the expressions with elliptic integrals (see the Appendix), and the resulting light curve $F = F(t)$ has been obtained and analyzed.

3. NUMERICAL RESULTS

Figure 2 shows the images of a source orbiting on an orbit with eccentricity $e = 0$ observed by the observer at infinity. The thick solid lines give the direct images and the thin lines the first-order images. The dashed circles refer to $B = 2m$ (m is the mass of the black hole) and give the scale. Figures (2a) and (2b) represent the cases with inclination $i = 80°$ and semimajor axes $a = 20m$ and $10m$. Figures 2c and 2d represent the same parameters as Figures 2a and 2b, but with viewing angle $i = 0°$. We can see that for $i = 0°$, both the direct image and the first image exhibit exactly circular tracks, while for $i = 80°$ the images are highly deformed. For $i = 0°$, gravitation gives rise to a redshift of the energy of photons only, whereas for $i = 80°$, gravitational bending deforms the image. It is interesting to notice that when the orbit is viewed face-on ($i = 0°$), the track of the first-order image is always smaller than that of the direct image, as the impact parameter of the photon is always smaller. However, if the system is not face-on, the situation will vary when the orbiting source is in front of the black hole (see Figs. 2a and 2b). In the case of circular orbits, the images are symmetric with respect to the axis defined by the normal to the orbital plane. This is not true, however, when the central object is a rotating black hole (see Cunningham & Bardeen 1973). The rotation effect is prominent only for first order or higher order images. This suggests that if the equatorial plane is full of an optically thick material, e.g., there is a thin accretion disk, the higher order images are absorbed, and it will be difficult to determine from the symmetry of the observed direct image whether the central hole is a Kerr black hole or a Schwarzschild black hole.

Figure 3 gives the direct images of the orbiting sources on orbits with eccentricity $e = 0.5$. The dashed circles refer again to $B = 2m$. Figures 3a and 3b represent the cases of $i = 80°$ with $a = 20m$ and $10m$, respectively. Figures 3c and 3d represent the same semimajor axes but with $i = 0°$. When the
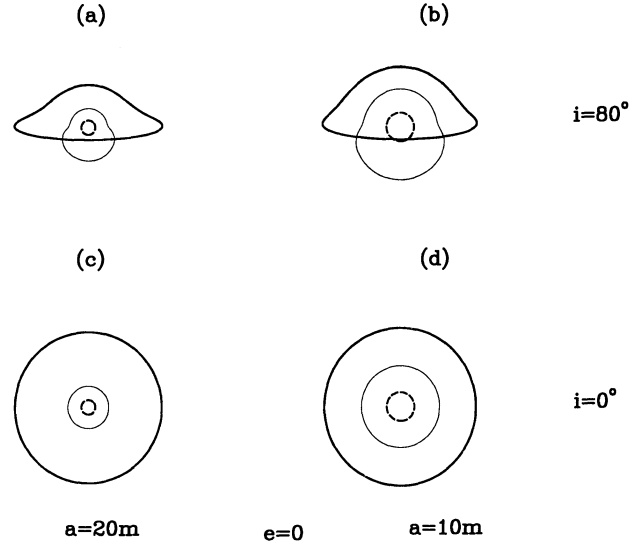

Fig. 2.—Direct and first-order images of circular orbits ($e = 0$) around a black hole. The thick solid lines give the direct images and the thin lines the first-order images. The dashed circles refer to $B = 2m$ and give the scale. (a) and (b) represent the cases in which the inclination $i = 80°$ and the semimajor axes $a = 20m$ and $10m$. (c) and (d) represent the same parameters as (a) and (b), but with viewing angle $i = 0°$.

orbiting source is on an eccentric orbit, its periastron advances and therefore the observed image is not closed, but one can still perceive many non-coinciding tracks. This is more evident in Figure 3c, where the periastron advance is $\sim 120°$, and so the path is rosetta-like. But in Figure 3d the periastron advance is much greater than $360°$, and consequently the source is spiraling from the pericenter to the apocenter and back.

Figure 4 gives the first-order images of the orbiting source for the same combinations of orbits and inclinations as Figure 3 ($e = 0.5$, $i = 80°$ or $0°$, and $a = 20m$ or $10m$). As in Figure 3, the images have different tracks for the same parameters, but when the inclination is $i = 0$, the images almost coincide.
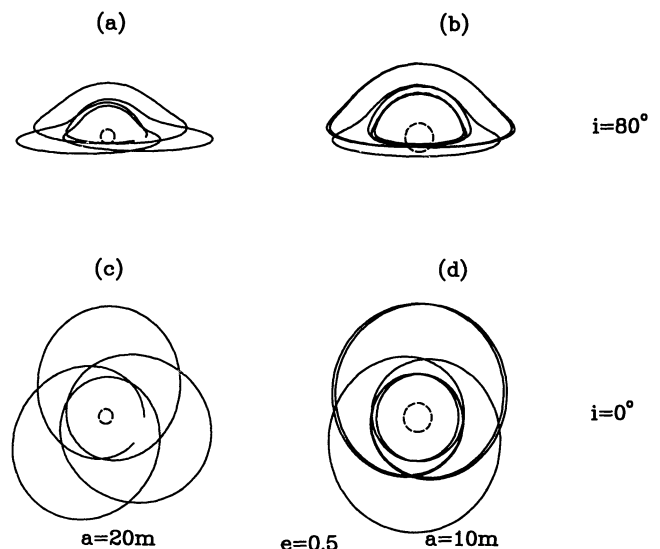

Fig. 3.—Direct images of eccentric orbits with eccentricity $e = 0.5$. The dashed circles refer again to $B = 2m$. (a) and (b) represent the cases of $i = 80°$ with $a = 20m$, $10m$, respectively. (c) and (d) represent the same semimajor axes but with $i = 0°$.
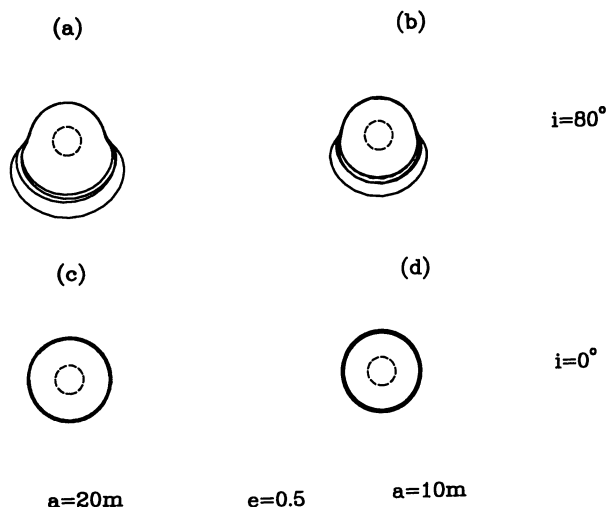
FIG. 4.—First-order images of eccentric orbits with eccentricity $e = 0.5$. The dashed circles refer again to $B = 2m$. (a) and (b) represent the cases of $i = 80°$ with $a = 20m$ and $10m$, respectively. (c) and (d) represent the same semimajor axes but with $i = 0°$.

Figure 5 shows the light curves (the flux is plotted in magnitudes and the time in units of the anomalistic period) for eccentricity $e = 0$ (Fig. 5a), $e = 0.5$ (Fig. 5b), the semimajor axis $a = 30m$ and the orbit inclination $i = 80°$. The solid lines refer to light curves due to direct images, the dashed lines stand for respectively the first-, the second-, and the third-order images. The higher order image contains lower energy. In the light curve of the direct image, there exists a hump and a peak in one period. The peak is due to gravitational lensing when the source is right behind the black hole, whereas the hump results from the Doppler effect when the orbiting source moves

toward the observer. In each sidereal period, the higher order images have two peaks corresponding to the lensing in conjunctions of the source with the black hole, i.e., the source is either behind or in front of the black hole. The Doppler effect is minute for higher order images of circular orbits, as the photons must be emitted almost perpendicularly to the direcion of the source motion, but it can be quite noticeable in the case of eccentric orbits. The lensing peaks in both the direct and the higher order images are shifted and the Doppler modulation distorted as the eccentricity increases, due to the varying velocity in the eccentric orbit. Moreover, the distortions evolve from one sidereal period to another because of the periastron advance.

The features of relativistic light curves are even more prominent for closer orbits, as seen in Figure 6. This figure shows the light curves for eccentricity $e = 0.5$, the semimajor axes $a = 20m$ for Figures 6a and 6c, $a = 10m$ for Figures 6b and 6d, the orbit inclination $i = 80°$ for Figures 6c and 6d, and $i = 30°$ for Figures 6a and 6b. The solid line refers to the light curve due to the direct image, and the dashed line the first image.

The Fourier analysis is the basic means to handle an observed signal with rapid variability, because it can reveal its multiperiodicity or quasi-periodicity. It has been shown (Bao 1992) that the above-mentioned features in the light curves of an individual spot on a circular orbit strengthen the higher harmonics of the orbital frequency and that this effect generates a characteristic hump in the power spectrum of the composite light curve of many randomly distributed spots due to the lack of spots inside the marginally stable circular orbit. The effect is even more complicated in the case of eccentric orbits where even the signal of an individual source is only quasi-periodic. The differences between the power spectra for sources with the same semimajor axis but different eccentricities can be seen in Figure 7. For $e = 0$, there are equally spaced δ-
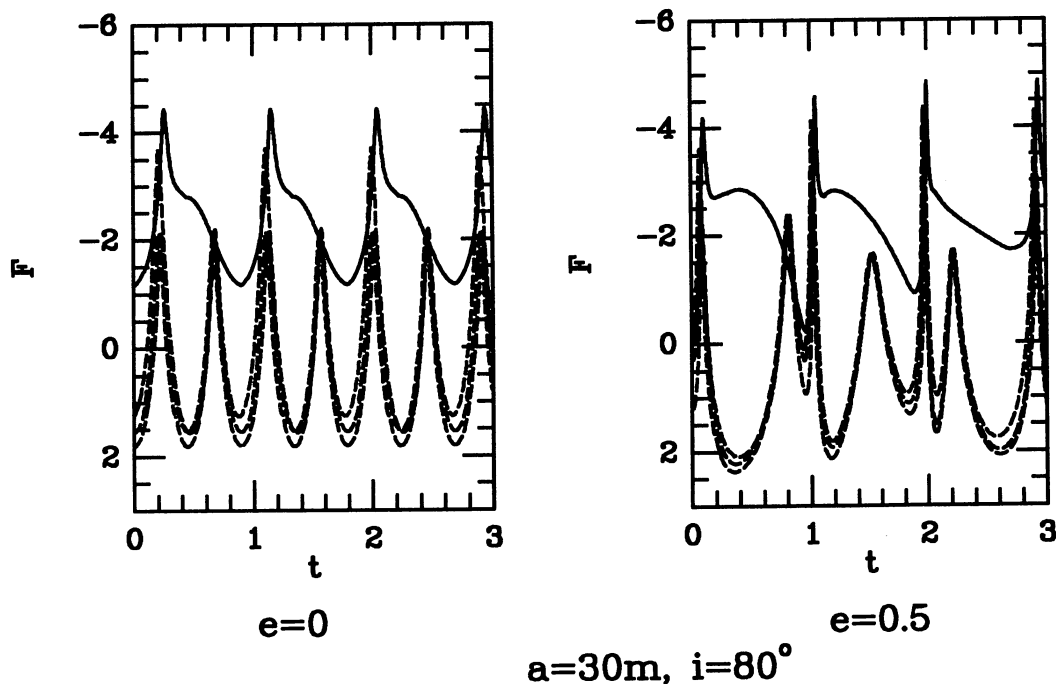

FIG. 5.—Light curves (the dependence of bolometric flux F in magnitudes on the photon arrival time in units of the anomalistic period of the orbiting source) of sources orbiting on circular and eccentric orbits with eccentricity (left) $e = 0$, and (right) $e = 0.5$. The semimajor axis is $a = 30m$ and the orbit inclination is $i = 80°$. The solid lines refer to light curves due to direct images, and the dashed lines stand for respectively the first-, the second-, and the third-order images.
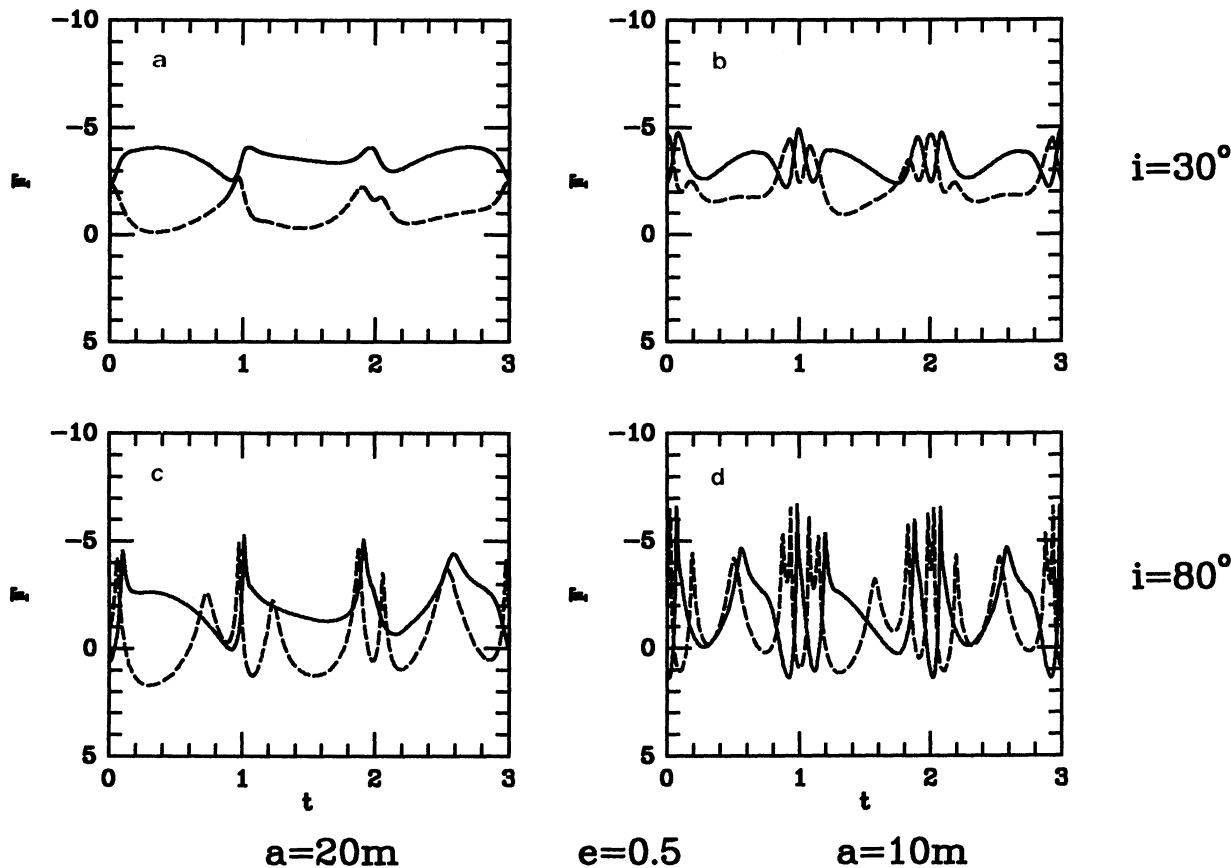
FIG. 6.—Light curves of eccentric orbits with eccentricity $e = 0.5$. The semimajor axes are (a and c) $a = 20m$ and (b and d) $a = 10m$. The orbit inclination is $i = 80°$ for (c) and (d), and $i = 30°$ for (a) and (b). The solid line refers to the light curve due to the direct image, and the dashed line the first image.

functions (smoothed by the sampling window) corresponding to the sidereal period and its harmonics. As eccentricity grows, the frequency of the sidereal orbit increases in comparison with
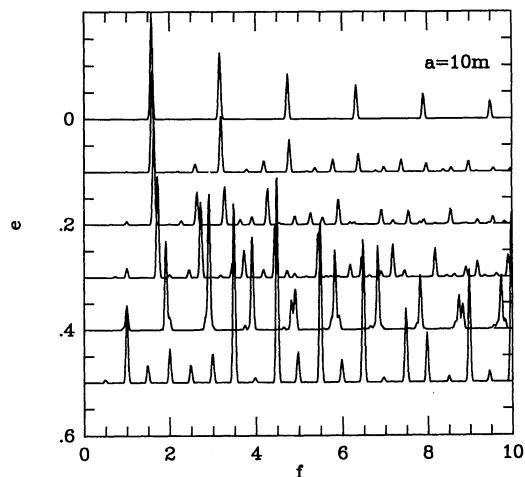

FIG. 7.—Power spectra F_f (in arbitrary units) of the light curves of sources on orbits with different eccentricities from $e = 0$ (top) to $e = 0.5$ (below). The step is chosen to be 0.1, the semimajor axis $a = 10m$ and the inclination of the orbit $i = 80°$. The frequency f is in units of frequency corresponding to the anomalistic period of the orbiting source.

the anomalous period used as the unit in the plot. Simultaneously, the higher harmonics are dumped (due to the varying shape of the light curve) and frequencies of beats with the anomalistic period begin to appear. For $e = 0.5$, the anomalistic frequency and its higher harmonics are the dominant features of the power spectrum. We are thus tempted to argue that the power spectrum of the light curve corresponding to many sources with randomly distributed semimajor axes and eccentricities can differ substantially from that due to circular orbits only. Moreover, this power spectrum can evolve in time due to secular changes of orbital parameters and/or the selective capture (or tidal disruption) of sources with small values of a and large values of e by the central black hole.

4. DISCUSSIONS

To the best of our knowledge, this is the first time that the images due to an orbiting source on an eccentric orbit have been presented. The shape of the images of the orbit depends strongly on gravity. Our results show that the image originating from an optically thick accretion disk alone would not enable us to distinguish between a Kerr black hole and a Schwarzschild black hole, whose images as well as shapes of light curves are similar. Unlike the circular orbit, the image of the orbiting source on an eccentric orbit is not closed, due to the relativistic advance of the periastron.

The light curve will not show exact periodicity if the orbit has a nonzero eccentricity, due to the periastron advance. In the light curves of the direct images gravitational lensing pro-

1994ApJ...425...63B

duces one peak in one period, while for the higher order images gravitational lensing leads to double peaks. Again the shape of the light curves depends very much on both the semimajor axis and the eccentricity of the orbit. Our calculations show that the energy contained in the light curves of higher order images is sometimes comparable with that contained in the light curves of the direct image (see Fig. 6).

For highly eccentric orbits, the power spectrum of the light curve does not show equally spaced peaks, and the main peaks in the spectra depend on the eccentricity of the orbit, which has practical implications for interpreting some important AGN phenomena. Recently, Papadakis & Lawrence (1993) found quasi-periodic oscillations in five *EXOSAT* observations of the Seyfert galaxy NGC 5548. It is interesting to note that the quasi-periodic frequency in the variability power spectrum varies in time. If the oscillation arises from the orbital motion, then the source cannot be on a stable circular orbit. One can well imagine that the oscillation may be due to a bright X-ray source on an eccentric orbit. As the source moves, the eccentricity of the orbit changes, as the object releases its energy and loses angular momentum, resulting in a change in the main peaks of the variability power spectrum. This might be a potential explanation for NGC 5548. Further work related to the issue will be carried out.

APPENDIX

The equations of geodesic motion in the Schwarzschild metric for both the source and the photon read

$$t = \frac{r}{r-2} E , \tag{A1}$$

$$\dot{r} = \left[E^2 - \frac{r-2}{r} (\mu + r^{-2}L^2) \right]^{1/2} , \tag{A2}$$

$$\dot{\vartheta} = r^{-2}(L^2 - \Phi^2/\sin^2 \vartheta)^{1/2} , \tag{A3}$$

$$\dot{\varphi} = r^{-2}\Phi/\sin^2 \vartheta , \tag{A4}$$

where μ is the mass of the test particle ($\mu = 0$ or 1 corresponds to photon and emitting matter, respectively), E, L, and Φ are the standard constants of motion.

For the source of radiation, $\mu = 1$, $\vartheta = \pi/2$, and $L = \Phi$. If the motion starts at $t = 0$ from the pericenter $r = r_p$ at $\varphi = \omega + \pi/2$, where ω is the longitude of the periastron, to the apocenter $r = r_a$, we can solve L and E from equation (A2) with the condition $\dot{r} = 0$ at the turning points $r_{p,a}$,

$$L_s = \left[\frac{a^2(1-e^2)^2}{a(1-e^2)-3-e^2} \right]^{1/2} \tag{A5}$$

$$E_s = \left\{ \frac{(a-2)^2 - a^2e^2}{a[a(1-e^2)-3-e^2)]} \right\}^{1/2} , \tag{A6}$$

where $a = (r_p + r_a)/2$ is the semimajor axis and $e = (r_a - r_p)/(r_p + r_a)$ is the eccentricity of the orbit (the subscripts "s" refer to the source of radiation). Equation (A4) can then be integrated (see, e.g., Chandrasekhar 1983) in the explicit form

$$\begin{aligned}
\varphi_s &= \int_{r_p}^{r_s} \left[\frac{E^2}{L^2} - \left(1 - \frac{2}{r}\right)\left(\frac{1}{L^2} + \frac{1}{r^2}\right) \right]^{-1/2} \frac{dr}{r^2} \\
&= \int_0^v \frac{a^{1/2}(1-e^2)^{1/2}}{\Delta(v)} dv \\
&= -2 \frac{a^{1/2}(1-e^2)^{1/2}}{\Delta(\pi)} \left[F\left(\frac{\pi - v}{2}, k\right) \right]_0^v ,
\end{aligned} \tag{A7}$$

where v is the true anomaly related to r by the transformation

$$r = \frac{a(1-e^2)}{1 + e \cos v} , \tag{A8}$$

$$\Delta(v) = [a(1-e^2) - 6 - 2e \cos v]^{1/2} , \tag{A9}$$

$F(x, k)$ is the elliptic integral of the first kind and

$$k = \frac{2e^{1/2}}{\Delta(\pi)} . \tag{A10}$$

Similarly integrating equation (A1), the coordinate time spent by the source in reaching the event of emission from the pericenter can be obtained in its explicit form (see also Vokrouhlický & Karas 1993), i.e.,

$$
\begin{aligned}
t &= \int_{r_p}^{r} \left[1 - \left(1 - \frac{2}{r}\right)\left(\frac{1}{E^2} + \frac{L^2}{E^2 r^2}\right) \right]^{-1/2} \frac{dr}{(1 - 2/r)} \\
&= \int_0^v \frac{a^2(1 - e^2)^{5/2}[(a - 2)^2 - a^2 e^2]^{1/2}\, dv}{(1 + e \cos v)^2 [a(1 - e^2) - 2 - 2e \cos v]\Delta(v)} \\
&= C_1 \left\{ \frac{1}{\Delta(\pi)} \left[F\left(\frac{\pi - v}{2}, k\right) \right]_0^v - C_2 \left[\frac{e \sin v \Delta(v)}{1 + e \cos v} + \Delta(\pi) E\left(\frac{\pi - v}{2}, k\right) \right]_0^v \right. \\
&\quad \left. - \frac{2}{a(1 - e)\Delta(\pi)} \left[(a + 3 + 4C_2)\Pi\left(C_3, \frac{\pi - v}{2}, k\right) + \frac{4}{a(1 + e) - 2} \Pi\left(C_4, \frac{\pi - v}{2}, k\right) \right]_0^v \right\},
\end{aligned}
$$
(A11)

where

$$ C_1 = a(1 - e^2)^{1/2}[(a - 2)^2 - a^2 e^2]^{1/2}, \tag{A12} $$

$$ C_2 = 1/[a(1 - e^2) - 4], \tag{A13} $$

$$ C_3 = 2e/(1 - e), \tag{A14} $$

$$ C_4 = 4e/[(1 - e)(2 - a - ae)]. \tag{A15} $$

Here,

$$ \Pi(n, x, k) = \int \frac{dx}{(1 + n \sin^2 x)\sqrt{1 - k^2 \sin^2 x}} \quad \text{etc.} $$

In the case of photons $\mu = 0$, hence the constants of motion E and L can be reduced to only one independent constant, the impact parameter $B = L/E$ (the orientation of the orbital plane gives the ratio of the angular momentum L and its projection Φ). The shape of the orbit can be expressed in terms of the polar angle ϕ in the plane of the photon motion as

$$ \phi = \int \frac{B\, du}{\sqrt{2u^3 B^2 - u^2 B^2 + 1}}, \tag{A16} $$

where $u = 1/r$. Following Bao (1992), three cases should be distinguished (see also Hadrava, Bao, & Østgaard 1993):

1. The trajectory has no turning point if

$$ \phi_\infty < \phi_{\rm crit} = \ln\left[\frac{(\sqrt{3} - 1)(\sqrt{3} + \sqrt{6/r_s + 1})}{(\sqrt{3} + 1)(\sqrt{3} - \sqrt{6/r_s + 1})} \right]; \tag{A17} $$

2. The trajectory has a turning point, but the photon does not pass through this point if

$$ \phi_{\rm crit} < \phi_\infty < \phi_{\rm turn}, \tag{A18} $$

3. The photon passes the turning point if

$$ \phi_{\rm turn} < \phi_\infty, \tag{A19} $$

where $\phi_{\rm turn}$ is ϕ_∞ for a photon which has its turning point ($\dot{r} = 0$) just at the radius $r = r_s$.

In cases (2) and (3), formula (A16) can be integrated explicitly in terms of elliptical integrals (see, e.g., Chandrasekhar 1983) by using the substitution ($r \to \chi$)

$$ \frac{p}{r} = 1 - \frac{qk^2}{2} \cos^2 \frac{\chi}{2}, \tag{A20} $$

where the pericenter distance p is the solution of the algebraic equation

$$ B^2 = \frac{p^3}{p - 2}; \tag{A21} $$

$$ q^2 = (p - 2)(p + 6); \tag{A22} $$

$$ k^2 = \frac{q - p + 6}{2q}. \tag{A23} $$

The corresponding expressions for ϕ_∞ read

$$ \phi_\infty = 2\left(\frac{p}{q}\right)^{1/2} [F(\chi_s/2, k) - F(\chi_\infty/2, k)]; \tag{A24} $$

$$ \phi_\infty = 2\left(\frac{p}{q}\right)^{1/2} [2K(k) - F(\chi_s/2, k) - F(\chi_\infty/2, k)]; \tag{A25} $$

for cases (2) and (3), respectively (χ_s and χ_∞ correspond to $r = r_s$ and $r \to \infty$). For all these cases, the light-travel time may also be calculated explicitly,

$$t = \int \left[1 - \left(1 - \frac{2}{r} \right) \frac{B^2}{r^2} \right]^{-1/2} \frac{dr}{1 - (2/r)}$$

$$= \int \frac{K_3 \, d\chi}{[1 + K_1 \sin^2 (\chi/2)]^2 [1 + K_2 \sin^2 (\chi/2)][1 - k^2 \sin^2 (\chi/2)]^{1/2}}$$

$$= K_3 \left[(q + p - 2) F \left(\frac{\chi}{2}, k \right) - 2q E \left(\frac{\chi}{2}, k \right) - q K_1 \frac{\sin \chi [1 - k^2 \sin^2 (\chi/2)]^{1/2}}{1 + K_1 \sin^2 (\chi/2)} + K_4 \Pi \left(K_1, \frac{\chi}{2}, k \right) + K_5 \Pi \left(K_2, \frac{\chi}{2}, k \right) \right], \quad (A26)$$

where

$$K_1 = - \frac{q - p + 6}{q - p + 2}, \tag{A27}$$

$$K_2 = - \frac{q - p + 6}{q + p + 2}, \tag{A28}$$

$$K_3 = - \frac{16 p (p - 2)^{1/2} q^{-1/2}}{(q - p + 2)^2 (q + p + 2)}, \tag{A29}$$

$$K_4 = - \frac{8 (p - 2)(q + p + 2)}{p(q + p - 2)}, \tag{A30}$$

$$K_5 = \frac{(q - p + 2)^2}{p}. \tag{A31}$$

The time t spent by the photon in reaching the observer (see eq. [A26]) differs for $r \to \infty$. What matters, however, is the relative delay between photons emitted from different parts of the orbit. We can thus express the time of the photon's arrival at the observer at infinity relatively to a reference photon emitted radially (i.e., with $B_{\rm ref} = 0$) from a point at a chosen radius $r_{\rm ref}$, i.e.,

$$\Delta t = \int_{r_{\rm em}}^\infty \left[1 - \left(1 - \frac{2}{r} \right) \frac{B^2}{r^2} \right]^{-1/2} \frac{dr}{1 - 2/r} - \int_{r_{\rm ref}}^\infty \frac{dr}{1 - 2/r}$$

$$= \int_{r_{\rm em}}^{r_{\rm ref}} \left[1 - \left(1 - \frac{2}{r} \right) \frac{B^2}{r^2} \right]^{-1/2} \frac{dr}{1 - 2/r} + \int_{r_{\rm ref}}^\infty \left\{ \left[1 - \left(1 - \frac{2}{r} \right) \frac{B^2}{r^2} \right]^{-1/2} - 1 \right\} \frac{dr}{1 - 2/r}. \tag{A32}$$

The second integral in this expression can be calculated by using the binomial expansion

$$\int_{r_{\rm ref}}^\infty \sum_{l=1}^\infty (-1)^l \binom{-1/2}{l} \left(\frac{B}{r} \right)^{2l} \left(1 - \frac{2}{r} \right)^{l-1} dr$$

$$= \left(\frac{B^2}{r} \left[\left[\frac{1}{2} + \frac{B^2}{r^2} \left\{ \frac{1}{8} - \frac{3}{16r} + \frac{B^2}{r^2} \left[\frac{1}{16} - \frac{5}{24r} + \frac{5}{28r^2} + \frac{B^2}{r^2} \left(\frac{35}{128} + \cdots \right) \right] \right\} \right] \right] + O(r^{-8}) \right)_{r = r_{\rm ref}}. \tag{A33}$$

If $r_{\rm ref}$ is chosen about one order greater than B (which is at maximum of the order of the apocenter distance $a(1 + e)$ of the orbit), it is sufficient to take into account a few terms in this expansion series, while the first integral is still a sufficiently small number varying significantly along the orbit (and hence the numerical inaccuracy from the subtraction of two almost equally large numbers can be avoided.

REFERENCES

Abramowicz, M. A., Bao, G., Fiore, F., Lanza, A., Massaro, E., & Perola, G. C. 1991a, in Physics of Active Galactic Nuclei, ed. W. J. Duschl & S. J. Wagner (Berlin: Springer), 61
Abramowicz, M. A., Bao, G., Lanza, A., & Karas, V. 1993, A&A, 272, 400
Abramowicz, M. A., Bao, G., Lanza, A., & Zhang, X.-H. 1989, in Proc. 23d ESLAB Symp., ed. J. Hunt & B. Battrick (Paris: ESLAB), 871
———. 1991b, A&A, 245, 454
Bao, G. 1992, A&A, 257, 594
Bao, G., & Stuchlík, Z. 1992, ApJ, 400, 163
Chandarasekhar, S. 1983, The Mathematical Theory of Black Holes (Oxford: Clarendon)
Cunningham, C. T. 1975, ApJ, 202, 788
Cunningham, C. T., & Bardeen, J. M. 1973, ApJ, 183, 237
Einstein, A. 1936, Science, 84, 506

Fabian, A. C. & George, I. M. 1990 in Iron Line Diagnostics in X-Ray Sources, ed. A. Treves, G. C. Perola, & L. Stella (Berlin: Springer), 169
Hadrava, P., Bao, G., & Østgaard, E. 1993, A&A, in press
Karas, V., Vokrouhlický, D., & Polnarev, A. G. 1992, MNRAS, 259, 569
Lightman, A. P. 1974, ApJ, 194, 429
Lightman, A. P., & Eardley, D. M. 1974, ApJ, 187, L1
Link, F. 1936, Comptes Rendus Acad. Sci. Paris, 202, 914
———. 1937, Bull. Astron., 10, 73
Misner, C. W., Thorne, K. S., & Wheeler, J. A. 1973, Gravitation (San Francisco: Freeman)
Papadakis, I. E., & Lawrence, A. 1993, Nature, 361, 233
Pineault, S. 1977, MNRAS, 179, 691

Pineault, S. 1980, ApJ, 241, 528
Pringle, J. E., Rees, M. J., & Pacholczyk, A. G. 1973, A&A, 29, 179
Sandip, K. C., & Bao, G. 1972, ICTP preprint
Shakura, N. I., & Sunyaev, R. A. 1976, MNRAS, 175, 613
Sikora, M., & Begelman, M. 1992, Nature, 356, 224
Stoeger, W. R. 1980, MNRAS, 190, 715
Vokrouhlický, D., & Karas, V. 1993, MNRAS, in press
Wiita, P. J., Miller, H. R., Carini, M. T., & Rosen, A. 1991, in Structure and Emission Properties of Accretion Disks, ed. C. Bertout et al. (Gif-sur-Yvette: Editions Frontières)
Zhang, X.-H., & Bao, G. 1991, A&A, 246, 21